

¹ **Estimating χ and K_T from fast-reponse thermistors on traditional shipboard**

² **CTDs: sources of uncertainty and bias.**

³ Andy Pickering*

⁴ *College of Earth, Ocean, and Atmospheric Sciences, Oregon State University, Corvallis, OR.*

⁵ Jonathan Nash

⁶ *College of Earth, Ocean, and Atmospheric Sciences, Oregon State University, Corvallis, OR.*

⁷ Jim Moum

⁸ *College of Earth, Ocean, and Atmospheric Sciences, Oregon State University, Corvallis, OR.*

⁹ Jen MacKinnon

¹⁰ *UCSD / Scripps Institute of Oceanography*

¹¹ *Corresponding author address: College of Earth, Ocean, and Atmospheric Sciences, Oregon State University, Corvallis, OR.

¹³ E-mail:

ABSTRACT

14 The acquisition of turbulence data from traditional shipboard CTD casts is
15 attractive, as it has the potential to dramatically increase the amount of deep-
16 ocean mixing observations globally. While data from shear-probes are eas-
17 ily contaminated by motion of the instrument platform, the measurement of
18 temperature gradient is relatively insensitive to vehicle vibration, making it
19 possible to measure temperature gradient from a shipboard CTD rosette. The
20 purpose of this note is to investigate the error and bias in estimating the rate of
21 dissipation of temperature variance χ and turbulent diffusivity K_T from tradi-
22 tional CTD casts. The most significant source of error is associated with the
23 fact that fast-response FP07 thermistors resolve only a fraction of the temper-
24 ature gradient variance at the fallspeed of typical CTD casts. Assumptions
25 must be made about the wavenumber extent of the temperature gradient spec-
26 trum, which scales with the rate of dissipation of turbulent kinetic energy, a
27 quantity that is not directly measured. Here we utilize observations from a
28 microstructure profiler to demonstrate the validity of the method of estimating
29 χ from thermistor data, and to assess uncertainty and bias. We then apply this
30 methodology to temperature gradient profiles obtained from χ -pods mounted
31 on a CTD (the CTD- χ -pod), and compare these to microstructure profiles ob-
32 tained almost synoptically at the equator. CTD- χ -pod estimates of χ compare
33 favorably to the direct microstructure measurements and demonstrate that the
34 χ -pod method is not significantly biased. This supports the utility of the mea-
35 surement as part of the global repeat hydrography program cruises, during
36 which this type of data has been acquired during the past few years.

³⁷ **1. Introduction**

³⁸ Turbulent mixing affects the distribution of heat, salt, and nutrients throughout the global ocean.

³⁹ Diapycnal mixing of cold, dense water with warmer water above maintains the abyssal overturning

⁴⁰ circulation (??), which affects global climate. Because the turbulence that drives mixing generally

⁴¹ occurs at scales that are not resolved in climate models, it must be parameterized, based on either

⁴² (i) aspects of the resolved model dynamics, (ii) through higher resolution models that capture the

⁴³ dynamics that feed energy to turbulence, or (iii) using other parameterizations that either dynami-

⁴⁴ cally or statistically quantify turbulent fluxes. Recent investigations have demonstrated that these

⁴⁵ models are sensitive to the magnitude and distribution of mixing (?). A comprehensive set of mea-

⁴⁶ surements that spans relevant dynamical regimes is needed to constrain mixing and develop more

⁴⁷ accurate parameterizations.

⁴⁸ Direct measurement of mixing with microstructure profilers equipped with shear probes is ex-

⁴⁹ pensive, time-intensive, and requires considerable care and expertise. Moreover, tethered profilers

⁵⁰ can't reach abyssal depths, requiring autonomous instruments to get deeper than \sim 1000-2000 m.

⁵¹ As a result, existing measurements of diapycnal mixing, especially in the deep ocean, are sparse

⁵² (?). In order to obtain estimates over a larger area, considerable work has gone into inferring mix-

⁵³ ing from measurements of the outer scales of turbulence, which are easier to obtain. One popular

⁵⁴ method is the use of Thorpe scales, where diapycnal mixing is inferred from inversions in profiles

⁵⁵ of temperature or density (??). The size of resolvable overturn is limited by the profiling speed

⁵⁶ and instrument noise (?). Several studies indicate relatively good agreement with microstructure

⁵⁷ and other observations, but there are some questions about the validity of the method and the as-

⁵⁸ sumptions made (??). Parameterizations based on profiles of shear and/or strain have also been

⁵⁹ developed and applied to estimate diapycnal mixing (?????). However, they rely on a series of as-

sumptions about the cascade of energy from large to small scales that are often violated; numerous studies (i.e., ? have shown that there is significant uncertainty associated with these parameterizations, in that there can be a consistent bias in a particular region, yet the sense of the bias (i.e., overpredict vs. underpredict) is not known a priori.

Quanitifying turbulence from velocity shear variance (to compute the dissipation rate of turbulent kinetic energy ε) is challenging on moorings or profiling platforms because there is usually too much vibration and/or package motion for shear-probes to be useful. Other methods (i.e., optics or acoustics) may hold some promise, but lack of scatterers often precludes this type of measurement, especially in the abyss. In addition, shear probes only provide ε , not the mixing of scalars, K , which is often inferred from ε by assuming a mixing efficiency Γ (?) as $K = \Gamma \varepsilon / N^2$, which N^2 is the buoyancy frequency. A more direct measure of the turbulent mixing is obtained from the dissipation rate of temperature variance χ (?). This has the advantage that (i) the temperature and temperature gradient can be computed and (ii) is relatively straightforawrd to measure, and (ii) the estimation of mixing from χ does not require assumptions about Γ . However, the spectrum of temperature gradient extends to very small scales, so that its spectrum is seldom fully resolved (and unlike shear variance, the wavenumber extent of the spectrum is not related to the amplitude of the temperature (or temperature gradient) spectrum). Assumptions about the spectral shape (Kraichnan vs. Bachelor, and the value of the “constant” q) and its wavenumber extent (governed by the Batchelor wavenumber $k_b = [\varepsilon / (v D_T^2)]^{1/4}$ (?)) are thus necessary to determine χ unless measurements capture the full viscous-diffusive subrange of turbulence (i.e., down to scales $\Delta x \sim 1/k_b \sim 1\text{mm}$), a criterion seldom achieved. To resolve this, we follow ? and ? and make the assumption that $K_T = K_\rho$ to determine the dissipation rate as $\varepsilon_\chi = (N^2 \chi) / (2\Gamma \langle dT/dz \rangle^2)$, permitting k_b to be estimated.

83 The goal of this paper is to outline and validate the methods used to compute χ and K_T with
84 χ -pods mounted on CTDs. We do this by applying our processing methodology to profiles of tem-
85 perature gradient measured by thermistors on the ‘Chameleon’ microstructure profiler, which pro-
86 vides a direct test of our methodology. Because Chameleon is a loosely tethered profiler equipped
87 with shear probes (Moum et al 1995), it directly measures ε and allows us to test our assumptions.
88 Specifically, it allows us to determine biases associated with computing chi from partially-resolved
89 temperature alone, as compared to that when it is computed by including knowledge of the dissi-
90 pation rate, which constrains the wavenumber extent of the scalar spectra. After establishing that
91 the method works, we then compare CTD- χ pod profiles to nearby microstructure profiles.

92 **2. Data**

93 *a. EQ14*

94 Data were collected on the R/V Oceanus in Fall 2014 during the EQ14 experiment to study
95 equatorial mixing. More than 2700 Chameleon profiles were made, along with 35 CTD-chipod
96 profiles bracketed by Chameleon profiles in order to maintain calibrations during the cruise. Most
97 Chameleon profiles were made to depth of about 250m, with CTD casts going to 500m or deeper.
98 The EQ14 experiment and results are discussed in more detail in (Buoyant gravity currents re-
99 leased from tropical instability waves, JPO (SJ Warner, RN Holmes, EH McHugh-Hawkins, JN
100 Moum) , in preparation).

101 **3. Methods**

102 As mentioned in the introduction, the temperature gradient spectrum is rarely fully resolved
103 down to the small scales of turbulent mixing. The fraction of the spectrum resolved depends on
104 the true spectrum (a function of χ and ε), the flowspeed past the sensor (‘fspd’), and the response

105 of the thermistor. The GE/Thermometrics FP07 thermistors we use typically resolve frequencies
 106 up to about 10-15 Hz. The maximum resolved wavenumber is then equal to $k_{max} = f_{max}/u$, while
 107 the wavenumber extent of the true spectrum varies with k_b (and $\varepsilon^{1/4}$). At the typical vertical fall
 108 rate of a CTD rosette ($\sim 1\text{m/s}$), only about 20% of k_b is resolved at $\varepsilon = 10^{-9}$ (Figure ??). While
 109 methods have been developed to fit the observed temperature gradient spectrum to theoretical
 110 forms (?), these work only when a large fraction of the temperature gradient spectrum is resolved.
 111 For the relatively high profiling speeds typical of CTD casts, we find these methods do not work
 112 well (see appendix for details) and therefore we use a different method.

113 We first outline our method for estimating χ , which relies on (i) determining the ?? instantaneous
 114 flowspeed past the sensor, (ii) identifying periods where the signals may be contaminated by the
 115 wake of the CTD rosette, (iii) defining the relevant N^2 and $(dT/dz)^2$, and (iv) JN: WHAT ELSE?...
 116 We then discuss some limitations and practical considerations that arise.

117 *a. Iterative Method for estimating χ*

118 For each ~ 1 second window, χ is estimated via the following procedure as outlined in ?. For
 119 isotropic turbulence,

$$\chi_T = 6D_T \int_0^\infty \Psi_{T_x}(k) dk \quad (1)$$

120 where D_T is the thermal diffusivity and $\Psi_{T_x}(k)$ is the wavenumber spectrum of dT/dx .

121 Note that dT/dx is not measured; dT/dt is measured, and dT/dx is inferred from Taylor's
 122 frozen flow hypothesis

$$\frac{dT}{dx} = \frac{1}{u} \frac{dT}{dt} \quad (2)$$

123 The wavenumber extent of the spectrum depends on the Batchelor wavenumber k_b , which is
 124 related to ε :

$$k_b = [\varepsilon / (v D_T^2)]^{1/4} \quad (3)$$

125 We assume that $K_\rho = K_T$ and $K_\rho = \Gamma \varepsilon / N^2$. Then dissipation rate is computed as

$$\varepsilon_\chi = \frac{N^2 \chi_T}{2\Gamma \langle dT/dz \rangle^2} \quad (4)$$

126 Typical thermistors do not resolve the spectrum out to k_b , so the measured spectrum is fit to the
127 Kraichnan form of theoretical scalar spectrum over the range of resolved wavenumbers ($k_{min} <$
128 $k < k_{max}$). The variance between the measured $[\Phi_{T_x}(k)]_{obs}$ and theoretical $[\Phi_{T_x}(k)]_{theory}$ spectra at
129 these wavenumbers is assumed to be equal:

$$\int_{k_{min}}^{k_{max}} [\Phi_{T_x}(k)]_{obs} dk = \int_{k_{min}}^{k_{max}} [\Phi_{T_x}(k)]_{theory} dk \quad (5)$$

130 An iterative procedure is then used to fit and calculate χ and ε :

131 1. First we estimate χ_T based on an initial guess of $\varepsilon = 10^{-7}$ Wkg $^{-1}$ and compute k_b . We
132 set $k_{max} = k_b/2$ or to a wavenumber equivalent to $f_{max} = 7$ Hz [i.e., $k_{max} = 2\pi(f_{max})/u$],
133 whichever is smaller. We choose $f_{max} = 7$ Hz because the thermistors' response rolls off at
134 higher frequencies (see appendix).

135 2. We then use Eq. (??) to refine our estimate of k_b and recompute χ_T using Eqs. (??) and (??).
136 3. This sequence is repeated and converges after two or three iterations.

137 Note that this procedure is equivalent to the explicit formulation of (?), except we use the Kraich-
138 nan spectrum.

139 *b. CTD- χ -pod Data Processing*

140 The basic outline for processing each CTD- χ -pod profile is as follows:

141 1. The correct time-offset for the χ -pod clock is determined by aligning dp/dt from the 24Hz
142 CTD data to vertical velocity calculated by integrating vertical accelerations measured by the

¹⁴³ χ -pod. χ -pod clock drift is small, typically on the order of 1 sec/week, but it is imperative to
¹⁴⁴ get records aligned within < 0.5 s so that the correct $u = w = dp/dt$ is used.

¹⁴⁵ 2. Low-order polynomial calibration coefficients are determined to convert thermistor voltages
¹⁴⁶ from χ pod to ITS90 temperature (as measured by the CTD). Figure ?? shows an example of
¹⁴⁷ the aligned and calibrated CTD- χ pod timeseries for one cast. Note the significant differences
¹⁴⁸ in amount of variance associated with the two sensors during down and up casts. For the
¹⁴⁹ upward-mounted sensor (T1), the downcast signal is entirely associated with the CTD wake,
¹⁵⁰ as is the upcast for the downward-mounted sensor. Only the ‘clean’ portions of the cast (e.g.,
¹⁵¹ the T1 upcast and the T2 downcast) are used in the χ pod calculations.

¹⁵² 3. Depth loops are identified and flagged in the 24Hz CTD data. χ -pod data during these times
¹⁵³ are discarded since the signals are likely contaminated by the wake of the CTD. Even for
¹⁵⁴ profiles that are significantly affected by ship heaving, good segments of data are obtained
¹⁵⁵ over a majority of the depths.

¹⁵⁶ 4. Buoyancy frequency N^2 and temperature gradient dT/dz are computed from 1-m binned CTD
¹⁵⁷ data.

¹⁵⁸ 5. Half-overlapping 1 sec windows of data are used to estimate χ , ε , and K_T following the
¹⁵⁹ methods described in ?, outlined in the previous section.

¹⁶⁰ c. *Example Spectra and Fits*

¹⁶¹ An example of the observed and fit spectra are shown in Figure ?? . Although only a small
¹⁶² portion of the spectrum is used in the fit, the method gives good results for χ . Errors in ε tend to
¹⁶³ be larger, due to additional assumptions required.

¹⁶⁴ d. flowspeed past the sensor

¹⁶⁵ The flowspeed past the thermistor is needed to convert the measured temperature derivative
¹⁶⁶ dT/dt to a spatial gradient. For the CTD- χ pod, the largest contribution to the flowspeed is usually
¹⁶⁷ the vertical velocity of the CTD package (dp/dt), which is close to 1m/s on average, so we typ-
¹⁶⁸ ically neglect the horizontal component of velocity in converting from frequency to wavenumber
¹⁶⁹ spectra. Although this will be a good approximation, errors may be introduced where horizontal
¹⁷⁰ velocities are large. Note that because it is the total instantaneous velocity magnitude that repre-
¹⁷¹ sents flow past the sesnor, neglecting the horizontal component of velocity (assuming $u = dp/dt$)
¹⁷² means we are always underestimating the true flowspeed past the sensor. When the CTD package
¹⁷³ is equipped with LADCP, the true flowspeed can be measured. In some cases (including EQ14)
¹⁷⁴ where the CTD was not equipped with LADCP, it would seem that the ship's ADCP could be
¹⁷⁵ used to estimate the horizontal component of velocity. However, because the CTD does not travel
¹⁷⁶ perfectly vertically in strong currents, this is difficult to do in practice. In a strong horizontal flow,
¹⁷⁷ the CTD will drift with the current while descending, lowering the flow relative to the sensors.
¹⁷⁸ On the upcasts, the CTD will be pulled against the current, increasing the flow relative to the sen-
¹⁷⁹ sors. Since the CTD in EQ14 was not equipped with LADCP, we use dp/dt as the flowspeed, and
¹⁸⁰ estimate potential errors in the appendix.

¹⁸¹ **4. Oceanographic Setting and Conditions**

¹⁸² Brief overview of dynamics in study region? More details are given in Warner et al (in prep).

183 **5. Results**

184 *a. Direct Test of χ pod Method*

185 We begin by utilizing the highly-resolved turbulence profiler data (for which both ε and χ are
186 measured) to test the assumptions of equation x in first perform a test of our method of estimating
187 χ . We first apply the χ pod method to each Chameleon profile, using only the FP07 thermistor
188 data. These results, which we will refer to as χ_χ , are then compared with χ_ε , computed by in-
189 tegrating the temperature gradient spectrum with k_b computed directly from shear-probe derived
190 ε . Qualitatively, χ_χ and χ_ε show very similar depth and time patterns (Figure ??), suggesting
191 the method generally works well. A more quantitative comparison is made with a 2-D histogram
192 (Figure ??), which shows that the two are well-correlated over a wide range of magnitudes.

193 *b. CTD χ -pod - Chameleon Comparison*

194 Having demonstrated that the method works for Chameleon data, we now compare χ from CTD-
195 mounted χ pods to χ_ε . In contrast to the Chameleon data, the CTD is more strongly coupled to
196 the ship, and therefore subject to more vibration, heaving, and artificial turbulence created by the
197 rosette. A total of 38 CTD- χ pod casts were done with Chameleon profiles immediately before
198 and after. We first compare CTD- χ pod profiles to the mean of Chameleon profiles bracketing
199 each cast, both averaged in 5m depth bins (Figure ??). The two appear to be correlated, with
200 considerable scatter. However, we expect significant natural variability even between Chameleon
201 profiles. Scatter plots of before/after Chameleon profiles (not shown), typically separated by about
202 an hour, show a similar level of scatter as the differences between methods, suggesting that the
203 observed differences (Figure ??) can be explained by natural variability in turbulence. This is
204 demonstrated by histograms of the ratio of χ from adjacent casts (Figure ??) which show that the

variability between CTD χ pod and Chameleon casts is similar to the natural variability between before/after Chameleon profiles. Average profiles from all CTD-Chameleon pairs (Figure ??) overlap within 95% confidence limits at all depths where there exists good data for both. Averages of subsets of profiles clustered in position/time (not shown) also agree.

6. Discussion

We have shown that χ can be accurately estimated from χ pods attached to CTD rosettes. The method also estimates ε , but we have not discussed it here since it involves more assumptions and uncertainties. One major assumption is the mixing efficiency Γ . A value of 0.2 is commonly assumed, but evidence suggests this may vary significantly. The χ pod method also assumes that $K_T = K_\rho$. Even if ε estimates have a large uncertainty, χ and K_T are robust and should be useful to the community.

The goal of CTD- χ pods is to expand the number and spatial coverage of ocean mixing observations. We have already deployed instruments during several experiments (IWISE, TTIDE) and on several GO-SHIP repeat-hydrography cruises. We plan to continue regular deployment on GO-SHIP and similar cruises, adding χ and K_T to the suite of variables measured and enabling scientists to explore relationships between these and other variables. The expanding database of mixing measurements from CTD- χ pods will also enable testing of other commonly-used or new mixing parameterizations. An example of data from a portion of the P16 GO-SHIP cruise is shown in Figure ??.

7. Conclusions

- The χ pod method was directly applied to temperature gradients measured by the Chameleon microstructure profiler on 2742 profiles during the EQ14 cruises. The estimated χ_χ agrees

227 well with χ_ε calculated using ε from shear probes over a wide range of magnitudes (Figure
228 ??).

- 229 • CTD- χ pod profiles were also compared to nearby Chameleon profiles during the cruise. Av-
230 eraged profiles of χ agree within 95% confidence limits. No bias was detected between the
231 estimates of χ .
- 232 • We conclude that estimates of χ and K_T from the CTD- χ pod platform are robust and reliable.

233 *Acknowledgments.* The EQ14 experiment was funded by ??. We thank the Captain and crew of
234 R/V Oceanus. Also thank people who helped collect the data, those who made the sensors, etc..

235 APPENDIX A

236 Sensitivity to flowspeed

237 We investigate the sensitivity of the χ pod calculations to flowspeed, which is used to convert
238 temperate gradient spectra from the frequency domain to the wavenumber domain via Taylor's
239 frozen flow hypothesis. In this data, we have ignored any horizontal velocities and assumed the
240 flow speed is equal to the vertical speed of the CTD rosette, determined from the recorded pressure
241 dp/dt . To test the sensitivity of the χ pod method to flowspeed, we repeated the calculations with
242 constant offsets added to the flowspeed. Since the total magnitude of velocity is used, dp/dt
243 is a minimum estimate of the true speed. Adding 0.1(1)m/s results in a median error of 13(52)
244 percent (Figure ??). Increasing the velocity tends to result in smaller values of χ , since it shifts
245 the spectrum to lower wavenumbers.

246 APPENDIX B

247 Sensitivty to Γ , N^2 and dT/dz

248 We investigated the sensitivity of the calculations to N^2 , dT/dz . The iterative method to estimate
249 chi requires the background stratification N^2 and temperature gradient dT/dz . We investigated the
250 sensitivity of the results to the choice of scale over which these are computed or smoothed. The
251 estimate of χ is insensitive to these scales. However, while dissipation rate ε and diffusivity K_T are
252 more strongly affected because they are linearly related to these values. Computing N^2 and dT/dz
253 over smaller scales results in larger values and hence some larger values of K_T .

254 APPENDIX C

255 **Test of MLE fitting method**

256 We tested the spectrum fitting method of ? and found that this method does not work well for
257 the χ_{pod} data, where only a small fraction of the spectrum is resolved. In particular, the MLE
258 method underestimates χ at larger magnitudes (Figure ??).

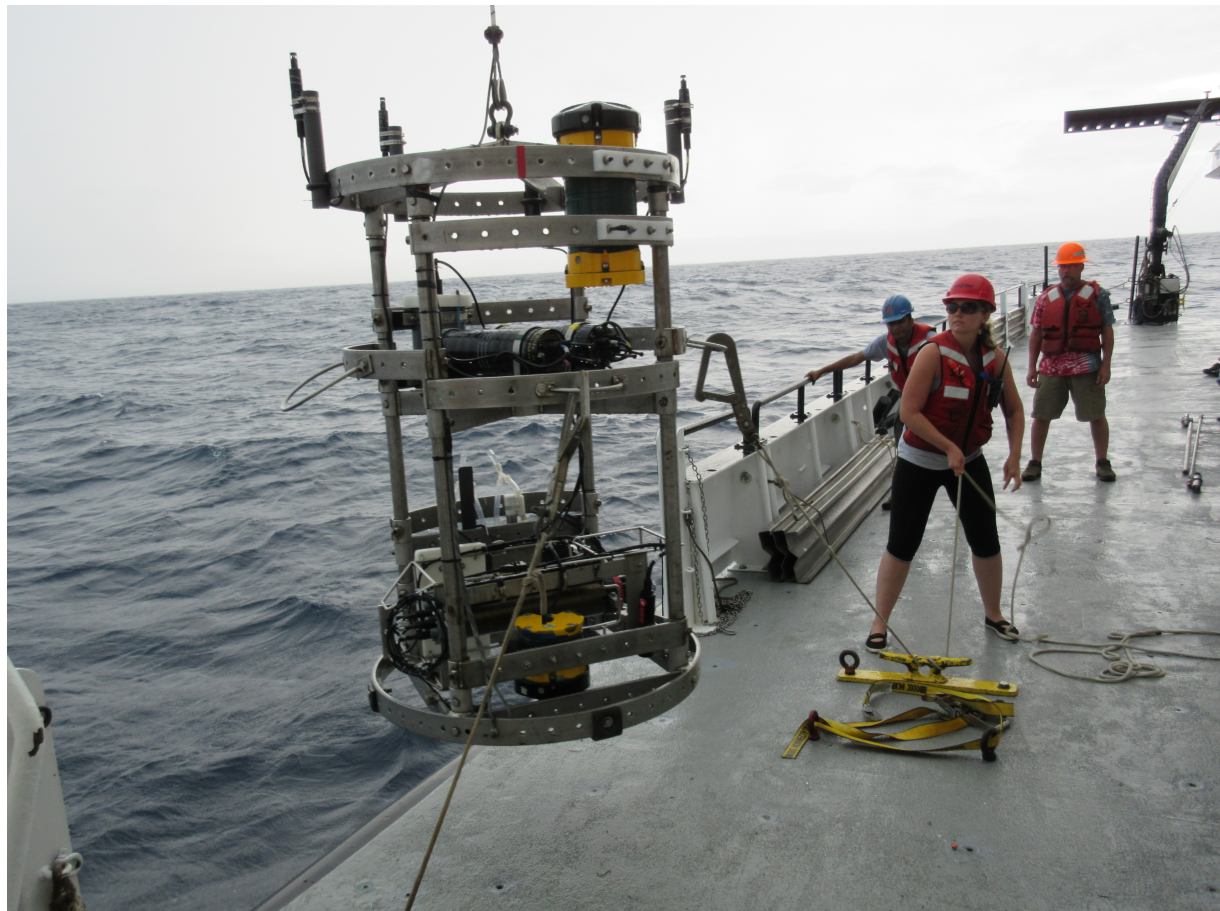
259 APPENDIX D

260 **Variability of thermistor transfer functions**

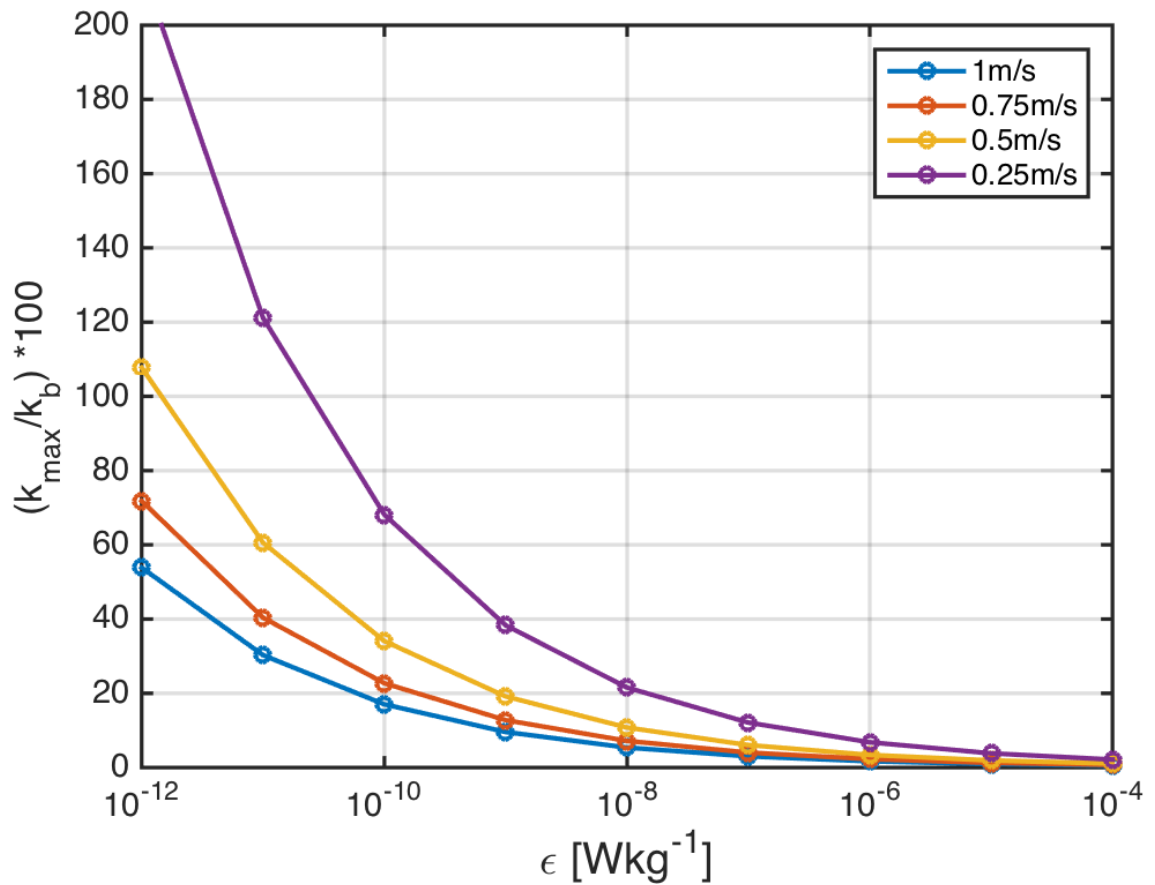
261 Measuring the transfer function for each individual thermistor proved too expensive and time-
262 consuming. We found that using only frequencies up to 7Hz (where the transfer function is equal
263 to or very close to unity) gives good agreement, and avoids the issue of the unknown transfer
264 functions. JN - I suggest you add the figure that shows the transfer functions for 10-20 thermistors,
265 and has a little histogram that convinces the reader that the variance is resolved
266 if one 7 Hz, but if you go out to 15-20 Hz, there is a large variability.

267 **LIST OF FIGURES**

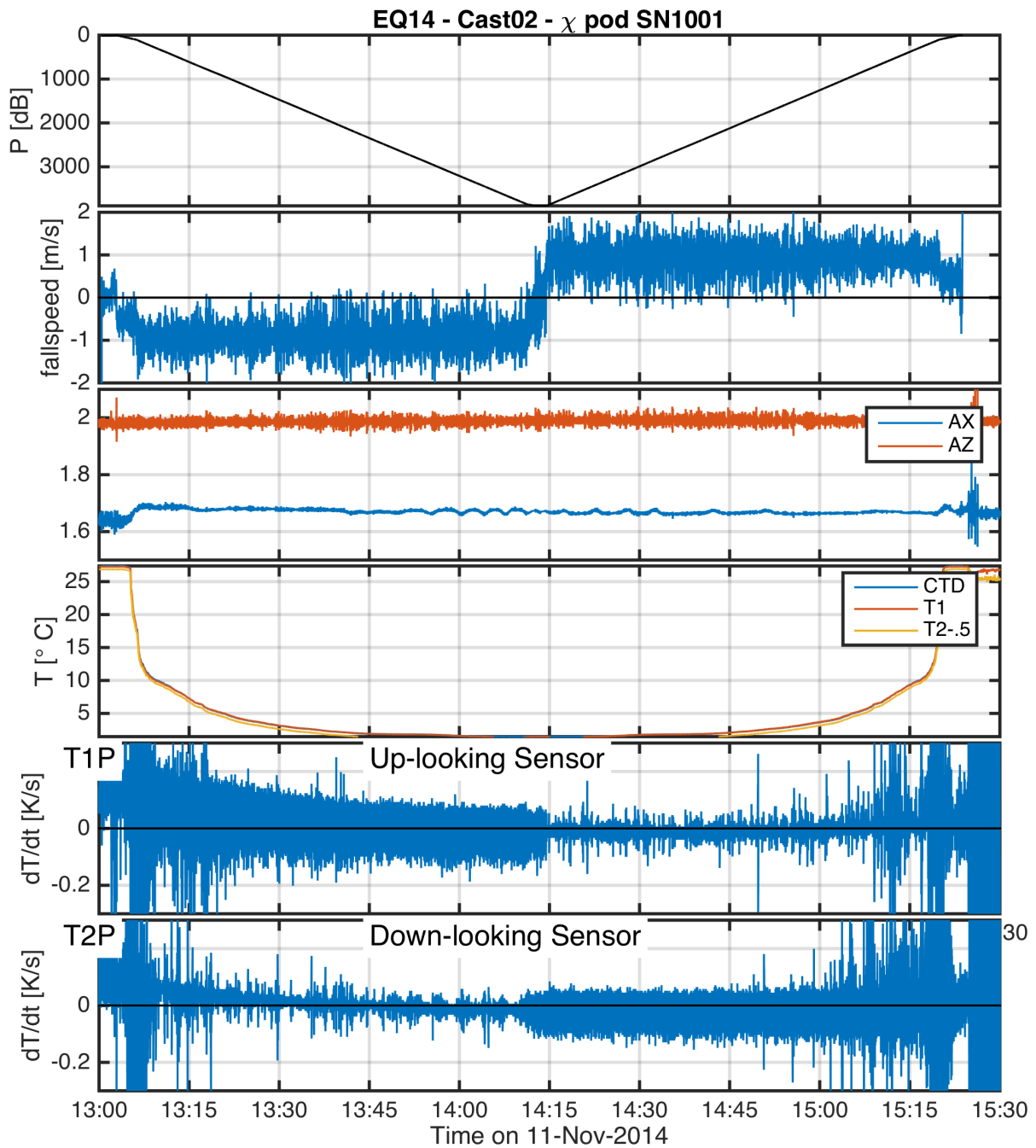
268 Fig. 1.	Photo of CTD rosette during EQ14 with χ -pods attached. ** Add close-up picture of mini-	16
269 chipod unit too**		
270 Fig. 2.	Ratio of the maximum observed wavenumber $k_{max} = f_{max}/u$ to the Batchelor wavenumber	17
271 k_b for different values of ε , assuming a $f_{max} = 7\text{Hz}$. Each line is for a different flowspeed.		
272 Fig. 3.	Example timeseries from one CTD cast during EQ14. a) CTD pressure. b) Fallspeed of	18
273 CTD (dp/dt) .c) Vertical and horizontal accelerations measured by χ -pod. d) Temperature		
274 from CTD and (calibrated) χ -pod sensors. T2 is offset slightly for visualization. e) Temper-		
275 ature derivative dT/dt measured by the upward-looking χ -pod sensor T1. f) Temperature		
276 derivative dT/dt measured by the downward-looking χ -pod sensor T2. **calibrate,add AX		
277 units. is it really -dT/dt? add 'up/down' looking labels for T' panels.		
278 Fig. 4.	Example temperature gradient spectra from EQ14. Solid black line show the observed spec-	19
279 tra. Dashed magenta line shows the fit theoretical Kraichnan spectra for the χ pod estimates.		
280 Purple line is Kraichnan spectra for Chameleon χ and ε . Vertical dashed blue lines indi-		
281 cate the minimum and maximum wavenumber used in the χ pod calculation. The Batchelor		
282 wavenumber k_b is also indicated by the cyan line.		
283 Fig. 5.	Depth-time plots of $\log_{10}\chi$ from both methods for EQ14 data. Top: χ pod method. Black	20
284 diamonds indicate casts used for comparison with CTD- χ pod profiles. Bottom: Chameleon.		
285 Fig. 6.	2D histogram of $\log_{10}(\chi)$ from Chameleon (x-axis) and χ pod method (y-axes). Values from	21
286 each profile were averaged in the same 5m depth bins.		
287 Fig. 7.	Histogram of the (left) ratio of the maximum observed wavenumber k_{max} to the Batchelor	22
288 wavenumber k_b , and (right) fspd for all profiles in EQ14.		
289 Fig. 8.	Scatter plot of χ from CTD- χ pod profiles versus the mean of bracketing Chameleon profiles.	23
290 Black dashed line shows 1:1, red are $\pm 10\chi$. **replace with histogram of ratios, or combine		
291 into one figure?**		
292 Fig. 9.	Histogram of \log_{10} of the ratio of χ for nearby casts. The first set is for the before	24
293 (cham1) and after (cham2) Chameleon profiles. the 2nd is CTD- χ pod profiles versus the		
294 before(cham1) profiles. The last is CTD- χ pod profiles versus the after(cham2) profiles.		
295 Dashed lines show the medians of each set. Note that bias is small/zero, and the variability		
296 between CTD/cham is similar to the natural variability between cham profiles.		
297 Fig. 10.	Time mean of χ for all CTD- χ pod - Chameleon cast pairs, with 95% bootstrap confidence	25
298 intervals.		
299 Fig. 11.	Example chipod data from P16N. Top: $dTdz$. Bottom: χ	26
300 Fig. 12.	Histogram of % error for χ computed with constant added to fallspeed, in order to examine	27
301 sensitivity to fallspeed.		
302 Fig. 13.	2D histograms of χ computed using the interative χ -pod method (top) and the MLE fit	28
303 (bottom) versus χ computed from Chameleon. Note that the MLE method underestimates		
304 χ at larger magnitudes.		



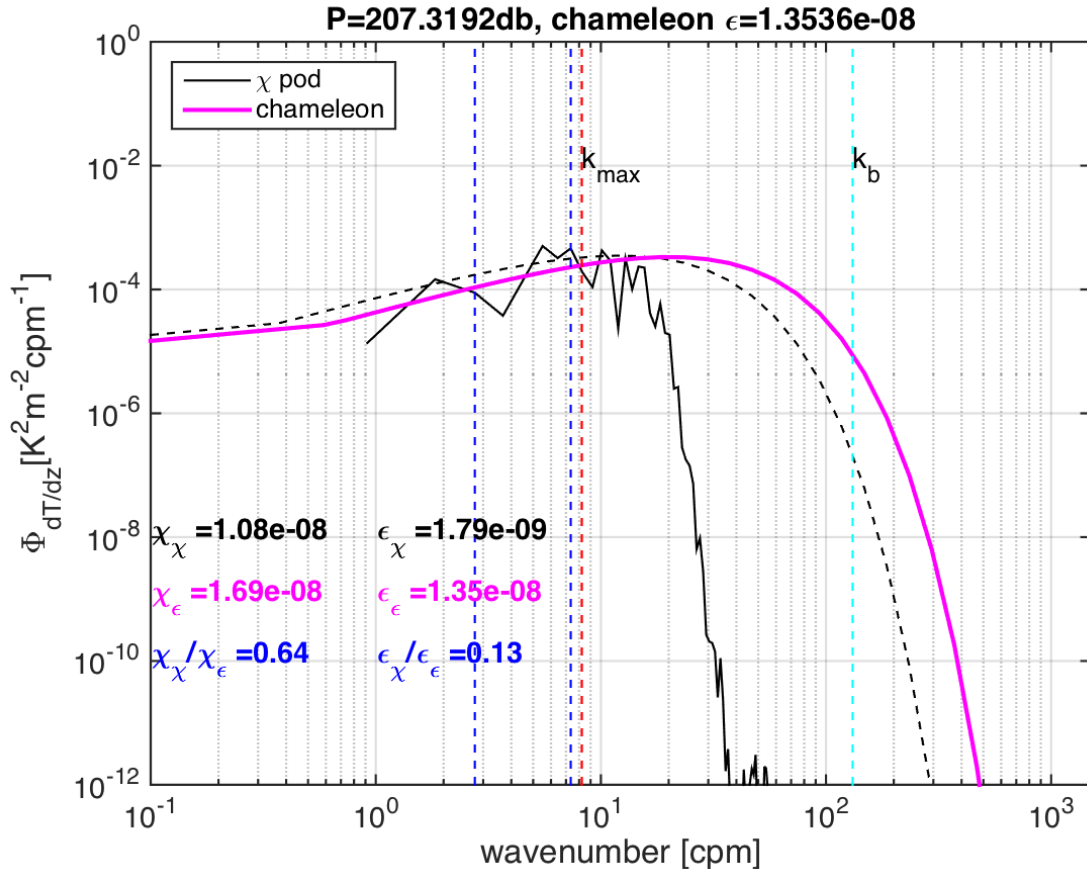
305 FIG. 1. Photo of CTD rosette during EQ14 with χ -pods attached. ** Add close-up picture of mini-chipod
306 unit too**



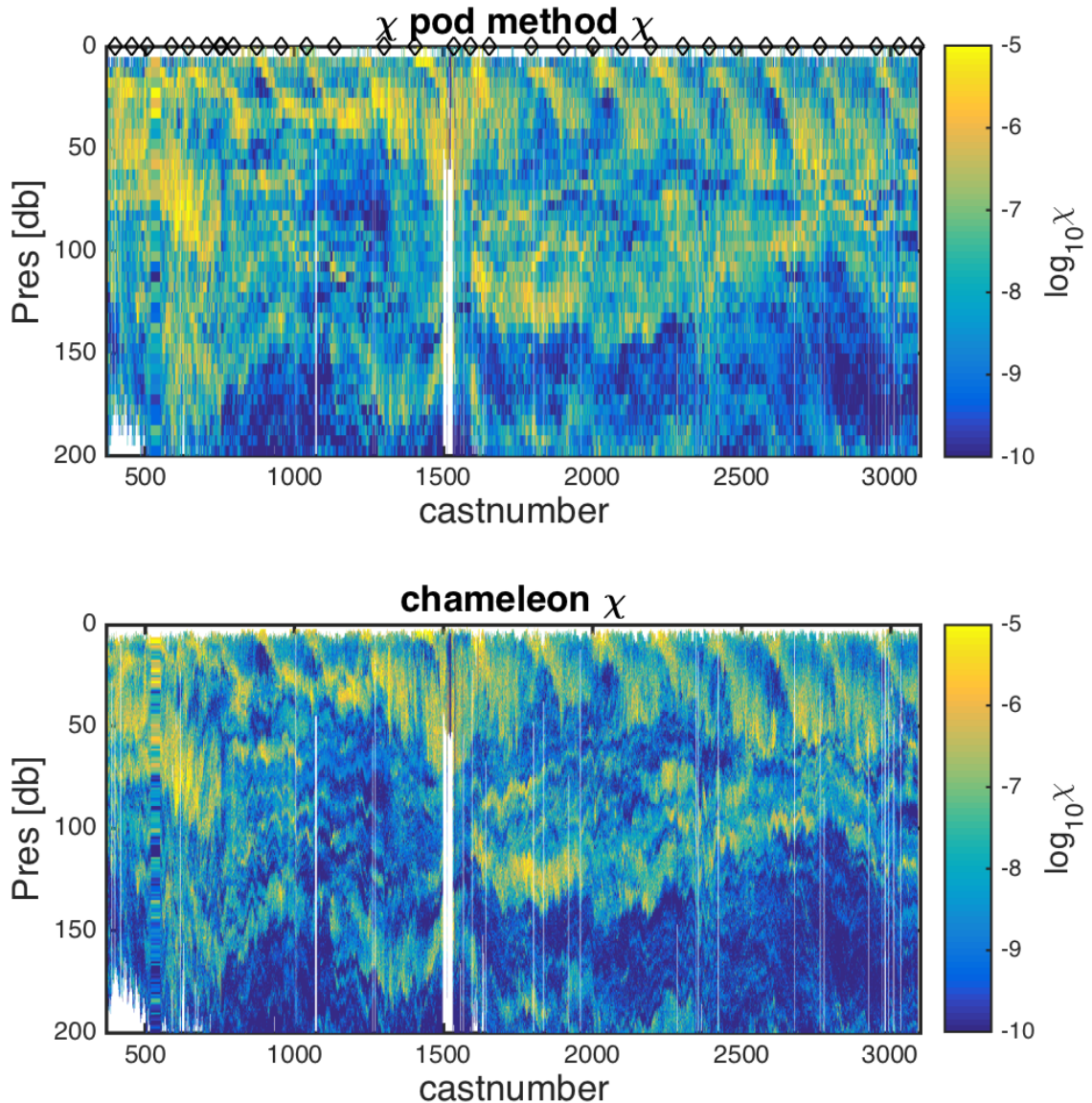
307 FIG. 2. Ratio of the maximum observed wavenumber $k_{\max} = f_{\max}/u$ to the Bachelor wavenumber k_b for
 308 different values of ϵ , assuming a $f_{\max} = 7\text{Hz}$. Each line is for a different flowspeed.



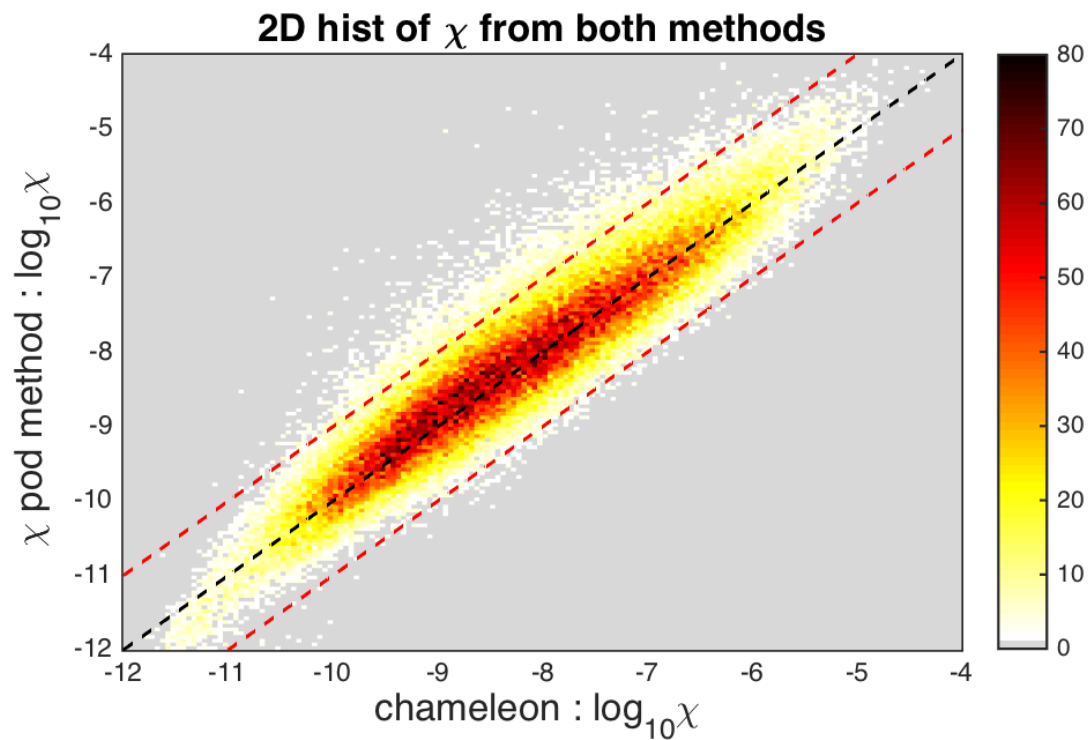
309 FIG. 3. Example timeseries from one CTD cast during EQ14. a) CTD pressure. b) Fallspeed of CTD (dp/dt)
 310 .c) Vertical and horizontal accelerations measured by χ -pod. d) Temperature from CTD and (calibrated) χ -pod
 311 sensors. T2 is offset slightly for visualization. e) Temperature derivative dT/dt measured by the upward-
 312 looking χ -pod sensor T1. f) Temperature derivative dT/dt measured by the downward-looking χ -pod sensor
 313 T2. **calibrate,add AX units. is it really $-dT/dt$? add 'up/down' looking labels for T' panels.



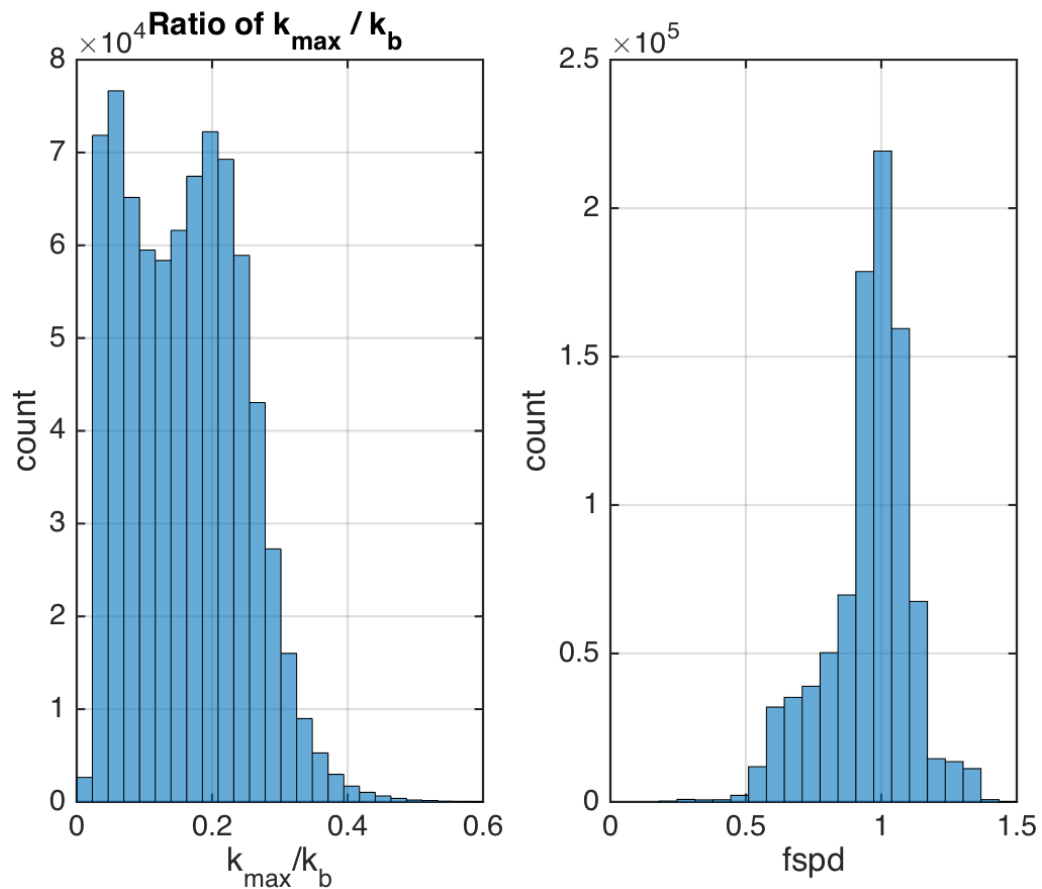
314 FIG. 4. Example temperature gradient spectra from EQ14. Solid black line show the observed spectra. Dashed
 315 magenta line shows the fit theoretical Kraichnan spectra for the χ pod estimates. Purple line is Kraichnan spectra
 316 for Chameleon χ and ϵ . Vertical dashed blue lines indicate the minimum and maximum wavenumber used in
 317 the χ pod calculation. The Batchelor wavenumber k_b is also indicated by the cyan line.



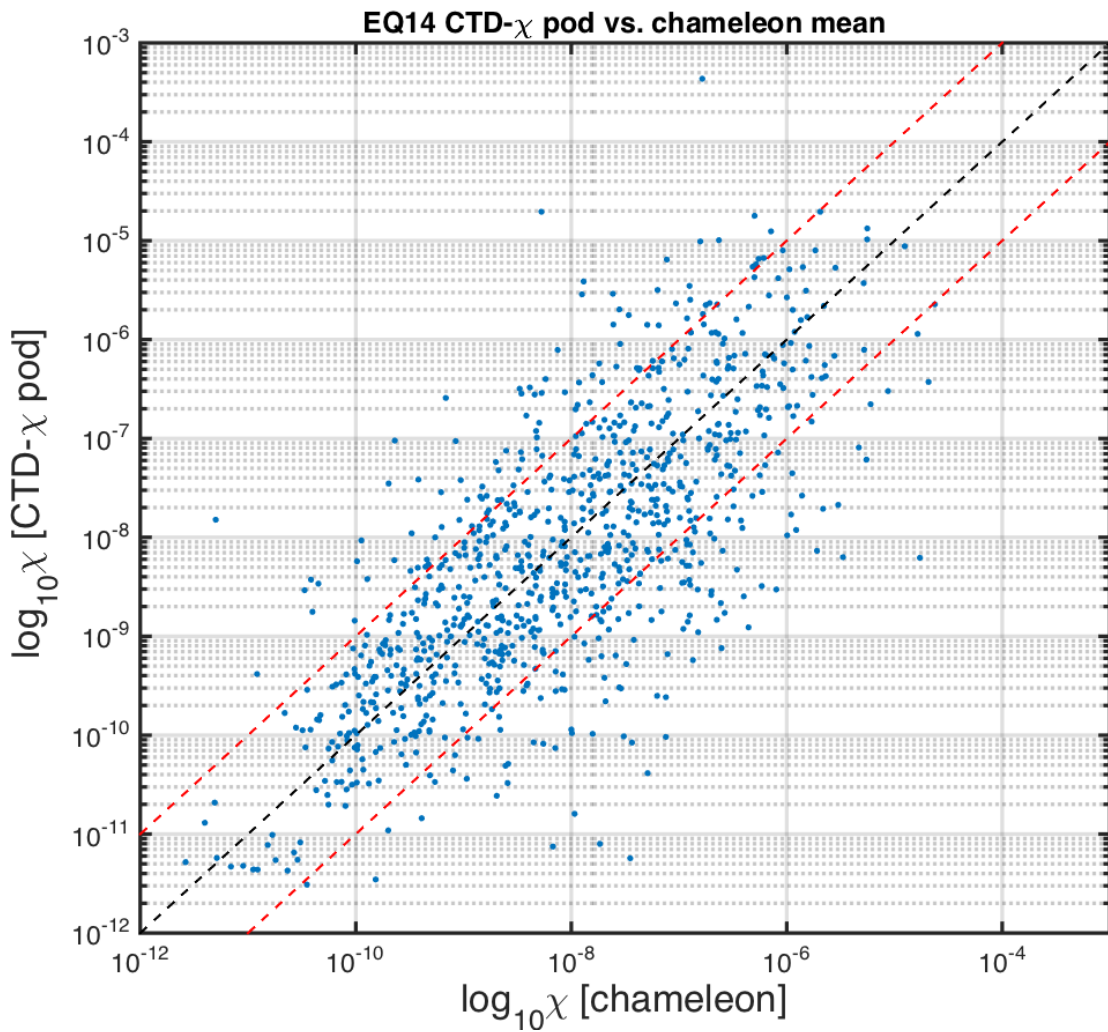
318 FIG. 5. Depth-time plots of $\log_{10} \chi$ from both methods for EQ14 data. Top: χ_{pod} method. Black diamonds
 319 indicate casts used for comparison with CTD- χ_{pod} profiles. Bottom: Chameleon.



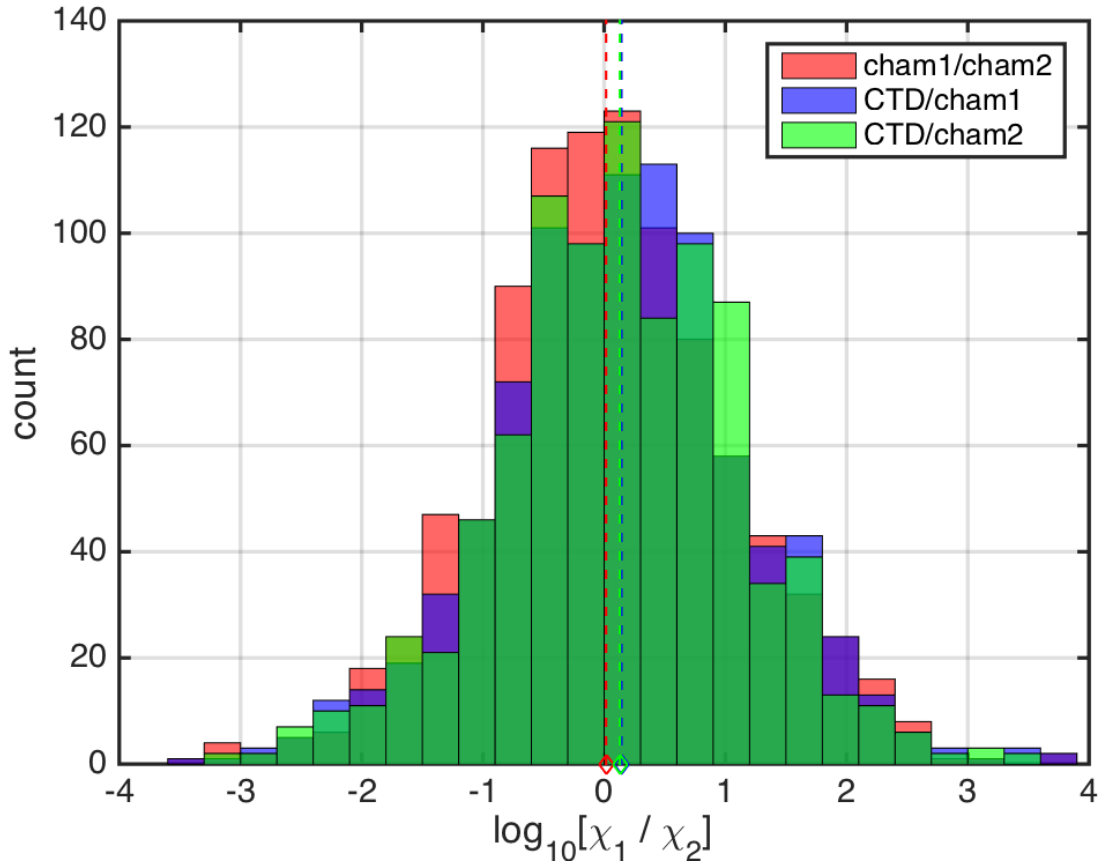
320 FIG. 6. 2D histogram of $\log_{10}(\chi)$ from Chameleon (x-axis) and χ_{pod} method (y-axes). Values from each
321 profile were averaged in the same 5m depth bins.



322 FIG. 7. Histogram of the (left) ratio of the maximum observed wavenumber k_{max} to the Bachelor wavenumber
 323 k_b , and (right) fspd for all profiles in EQ14.



³²⁴ FIG. 8. Scatter plot of χ from CTD- χ pod profiles versus the mean of bracketing Chameleon profiles. Black
³²⁵ dashed line shows 1:1, red are $\pm 10 \times$. **replace with histogram of ratios, or combine into one figure?**



326 FIG. 9. Histogram of \log_{10} of the ratio of χ for nearby casts. The first set is for the before (cham1) and
 327 after (cham2) Chameleon profiles. the 2nd is CTD- χ pod profiles versus the before(cham1) profiles. The last is
 328 CTD- χ pod profiles versus the after(cham2) profiles. Dashed lines show the medians of each set. Note that bias
 329 is small/zero, and the variability (spread) between CTD/cham is similar to the natural variability between cham
 330 profiles.

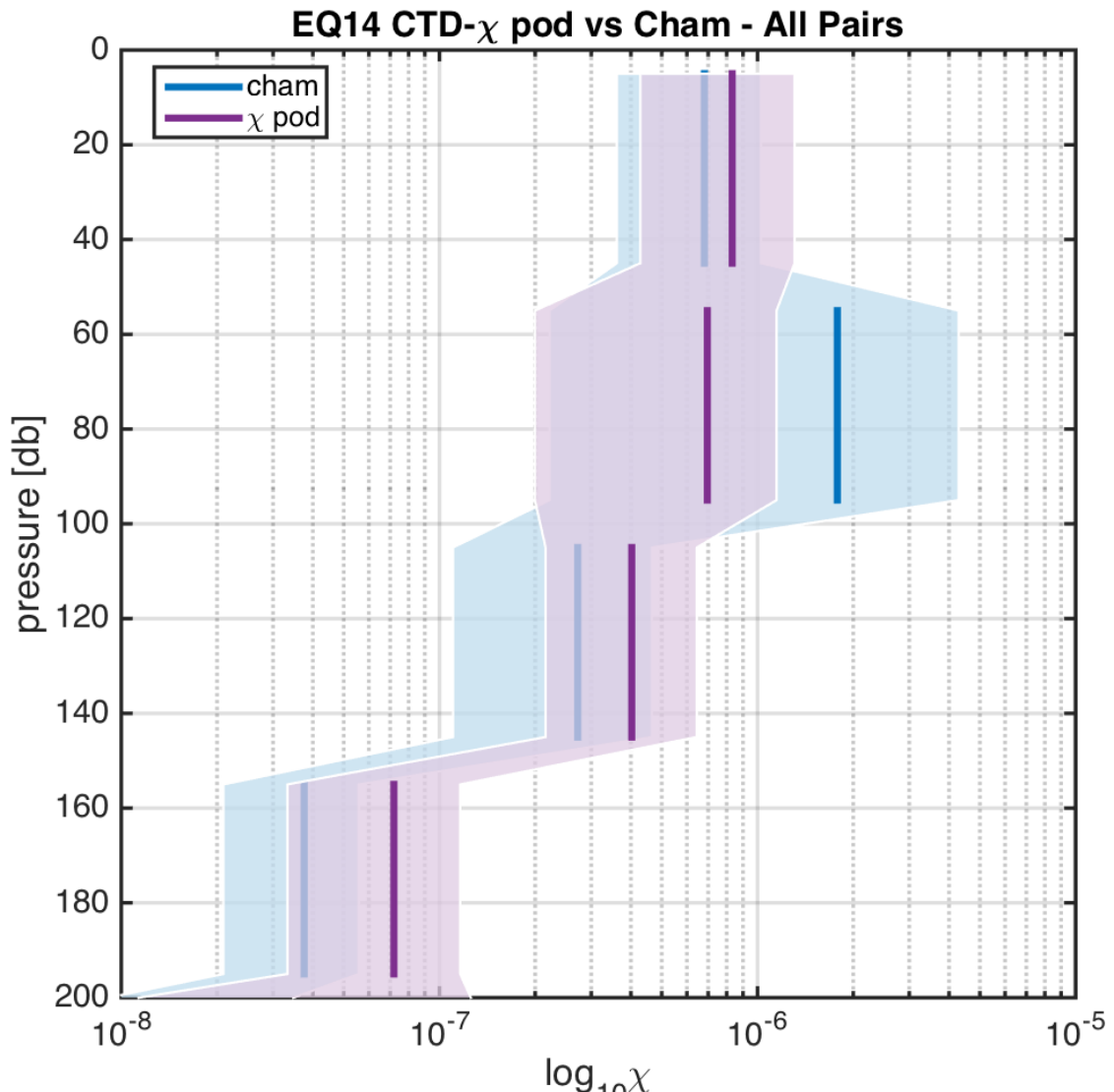


FIG. 10. Time mean of χ for all CTD- χ pod - Chameleon cast pairs, with 95% bootstrap confidence intervals.

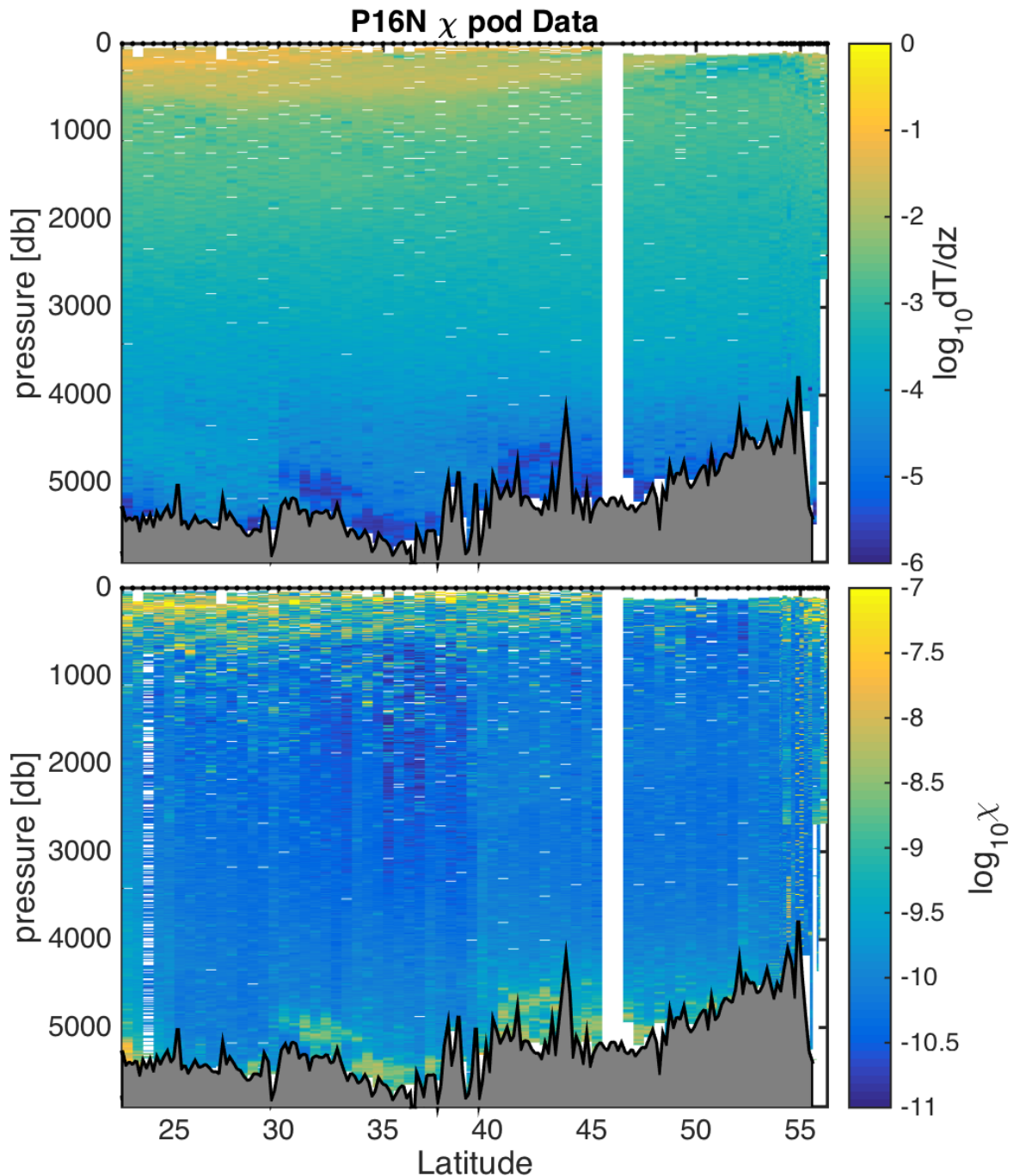
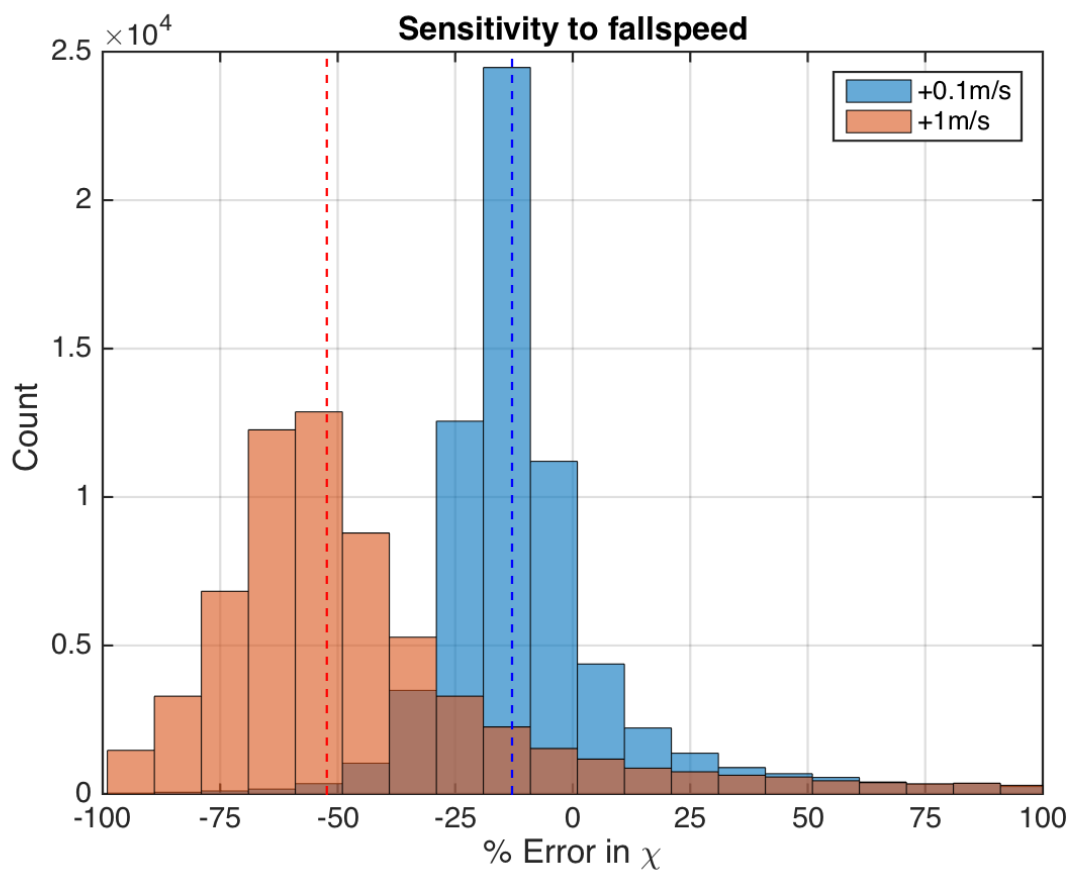
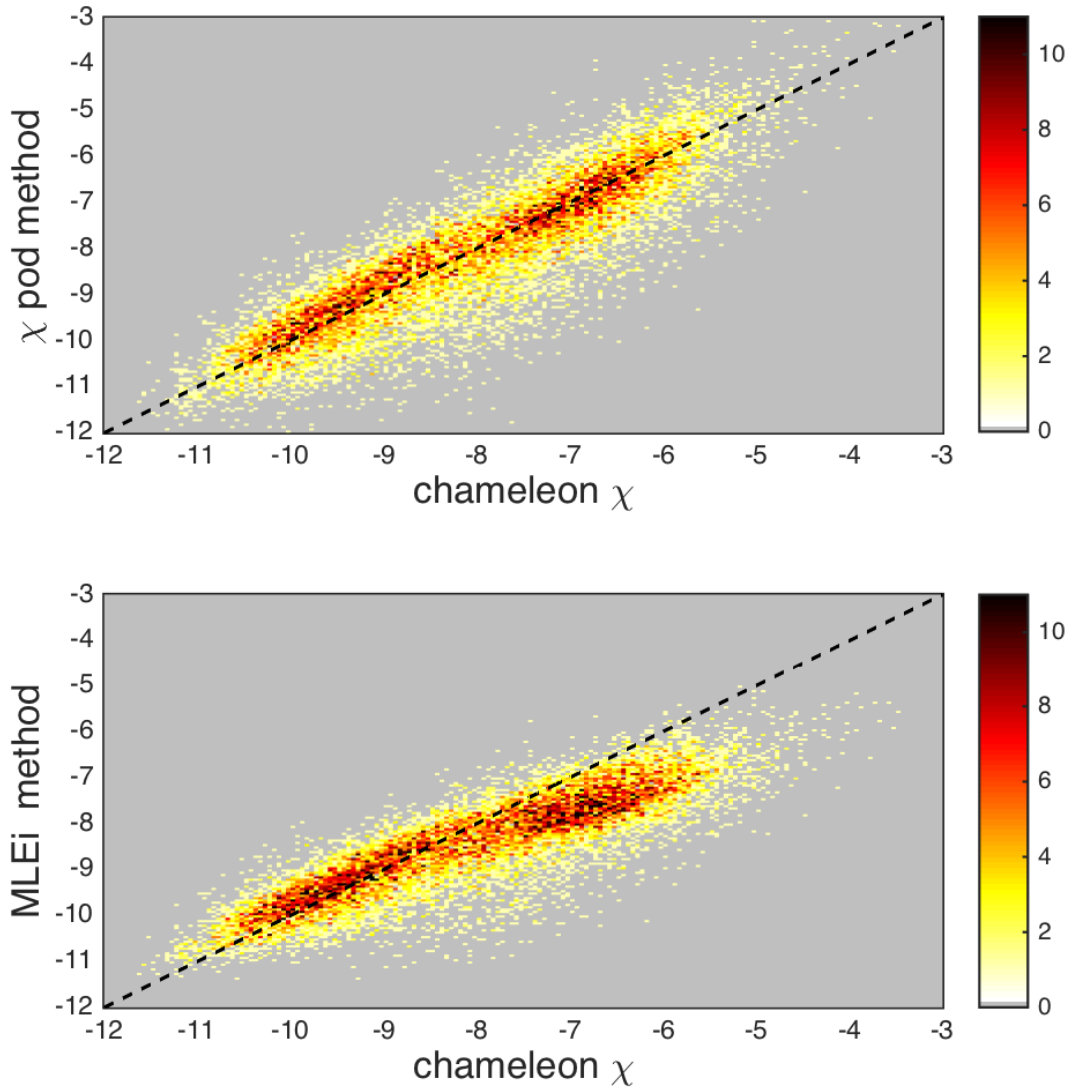


FIG. 11. Example chipod data from P16N. Top: $dTdz$. Bottom: χ .



331 FIG. 12. Histogram of % error for χ computed with constant added to fallspeed, in order to examine sensitivity
 332 to fallspeed.



333 FIG. 13. 2D histograms of χ computed using the interative χ -pod method (top) and the MLE fit (bottom)
 334 versus χ computed from Chameleon. Note that the MLE method underestimates χ at larger magnitudes.